Communications on Applied Nonlinear Analysis
ISSN: 1074-133X
Vol 32 No. 10s (2025)

A Precision-Enhanced Spectral Framework for Sturm–Liouville Eigenvalue Computation

P. Sri Harikrishna[1] , G. Sudheer[2]

[1]GITAM School of Science, GITAM (Deemed to be University), Visakhapatnam-530045, India
[2]Gayatri Vidya Parishad College of Engineering for Women, Visakhapatnam-530048, India

Article History:

Received: *02-11-2025*

Revised: *11-12-2025*

Accepted: *20-12-2025*

Abstract

Eigenvalue computation for Sturm–Liouville problems lies at the intersection of spectral approximation theory and high-accuracy scientific computing. Traditional Chebyshev differentiation matrix (CDM) approaches encounter three compounding difficulties: increasing discretization size, higher-order derivatives, and tightly clustered eigenvalues. These issues stem from the repeated matrix multiplications required to construct higher-order differentiation operators, which significantly amplify numerical round-off errors. As a result, accuracy deteriorates rapidly as the problem size and derivative orders grow, limiting the reliability of classical CDM-based implementations in demanding spectral regimes.

This paper presents a high-precision computational framework based on Chebyshev–trigonometric collocation (CTC) for solving Sturm–Liouville eigenvalue problems. The proposed approach avoids the conventional matrix-product assembly by directly evaluating derivative terms using closed-form trigonometric expressions at collocation nodes. This entry-wise construction significantly reduces numerical round off errors and improves computational stability. For higher-order problems, particularly fourth-order equations, multiple boundary conditions at each endpoint are handled using a node-reduction strategy. Although this approach increases the condition number with problem size, it consistently eliminates spurious eigenvalues across all tested resolutions, ensuring physically meaningful solutions. A rigorous theoretical analysis establishes geometric convergence of the method, supported by tools from spectral approximation theory, quadrature analysis, functional analysis, and operator perturbation theory. The convergence behavior is governed by the analytic properties of the problem coefficients, enabling highly accurate eigenvalue approximations. All computations are carried out in high-precision arithmetic using MATLAB, allowing the method to achieve extremely small error levels beyond the limits of standard double precision. This enables reliable verification of convergence and numerical accuracy. The effectiveness of the framework is demonstrated on six benchmark problems, including challenging cases with clustered spectra, variable coefficients, mixed boundary conditions, and applications to beam vibration models with both constant and spatially varying properties. The results confirm that the proposed method delivers high accuracy, robustness, and consistency across a wide range of Sturm–Liouville problems.

Keywords: Chebyshev spectral collocation; high-precision eigenvalue computation; Sturm–Liouville problems; fourth-order problems; geometric convergence; node-reduction; functionally graded beams; multiprecision arithmetic.

MSC 2020: 65N35, 34L15, 65N25, 41A25

1. Introduction

1.1 Physical and Mathematical Context

Sturm–Liouville problems occupy a foundational position in mathematical physics and engineering analysis. Since the classical contributions of Sturm [1] and Liouville [2], eigenvalue problems of this type have served as the backbone for modelling diverse physical

processes — wave propagation, heat conduction, vibrational mechanics, and quantum systems [3, 4]. In many settings, separation of variables applied to linear PDEs naturally produces a Sturm–Liouville structure, making accurate eigenvalue computation essential [5, 6]. The second-order self-adjoint form

$$-(p(x)\,y')' + q(x)\,y = \lambda\, w(x)\,y, \quad x \in [\alpha, \beta], \tag{1}$$

arises in quantum mechanics (Schrödinger operators), acoustics (vibrating strings and membranes), and heat transfer (radially symmetric problems) [3]. Its fourth-order counterpart

$$(p_2(x)\,y'')'' - (p_1(x)\,y')' + p_0(x)\,y = \lambda\, w(x)\,y \tag{2}$$

governs the transverse vibration of Euler–Bernoulli beams, buckling of columns, and wave propagation in elastically supported structures [33, 58]. The free-vibration equation of an exponentially functionally graded (EFG) beam — a contemporary structural model in which material properties vary continuously with spatial position— is a canonical example of the fourth-order form with variable, entire-function coefficients.

Although some SLPs admit closed-form eigenpairs, most practical models feature variable coefficients or higher-order structure. Numerical methods remain indispensable, and computing high-index eigenvalues poses significant challenges [1, 3]. Standard ODE solvers often deteriorate for high-index solutions, prompting the development of tailored approaches [7].

1.2 Background

Second-order SLPs have attracted a wide range of numerical approaches: finite-element formulations [8], quadrature-based schemes [9, 10], decomposition techniques [11], Chebyshev collocation [12, 13], wavelets [14], homotopy methods [15], Legendre–Galerkin–Chebyshev approaches [16], variational iteration [17], Hermite interpolation [18], sinc-Galerkin methods [19], polynomial expansion [20], high-index eigenfunction approximation [21], deep learning [22], perturbative approaches [23], and generalised SLP solvers [24].

Fourth-order SLPs are more demanding because four boundary conditions must be imposed — typically two at each endpoint. Oscillation theory methods [25], Fliess series [26], iterative methods [27, 28], sampling approaches [29, 30], matrix methods [31], differential quadrature [32], dynamic stiffness methods [33], eigenvalue computations [34], Bernoulli–Chebyshev methods [35], fractional pseudospectral approaches [36], and non-self-adjoint extensions [37] have all been proposed. Among spectral methods, pseudospectral collocation on Chebyshev nodes offers *geometric* (spectral) convergence for smooth problems [38, 39] and is particularly attractive [40]; the present work builds on this foundation.

1.3 The Three Failure Regimes of Standard CDM

Implementation of pseudospectral methods for high-order SLPs typically follows Fornberg [41] or the differentiation-matrices approach of Sadiq and Viswanath [42]. The standard procedure constructs the first-order Chebyshev differentiation matrix D_N via the Trefethen recurrence [39, Chapter 6] and forms higher-order matrices by repeated multiplication:

$$D_N^{(k)} = \underbrace{D_N \cdot D_N \cdots D_N}_{k \text{ times}}.$$

Taher et al. [5] used this approach for fourth-order SLPs; however, constructing $D_N^{(k)}$ by repeated multiplication is known to accumulate roundoff [42], with three distinct failure regimes that motivate the present framework:

1. **Large N:** Each multiplication of D_N amplifies rounding errors by a factor $O(N)$ per level, so $D_N^{(4)}$ accumulates $O(N^3\varepsilon_{\text{mach}})$ error per row for moderate-to-large N [42].
2. **High derivative order:** Fourth-order problems require $D_N^{(4)} = D_N \cdot D_N \cdot D_N \cdot D_N$, the worst case for matrix-product round-off [42]; entries of magnitude $O(N^8)$ combine small relative errors into large absolute errors for high-degree modes.
3. **Clustered spectra:** Near-degenerate eigenvalues — the Coffey–Evans triplets of Example 1 differ only in the ninth decimal place [1] — require residuals below 10^{-13}; at double precision the CDM error floor precludes their resolution, whereas the Chebyshev Trigonometric Collocation assembly retains full extended-precision fidelity.

1.4 Contributions of This Paper

The CTC framework addresses all three regimes through the following contributions:

(i) Entry-wise trigonometric assembly: Each entry $T_j^{(k)}(\cos\theta_i)$ is evaluated from the closed-form recursion generated by $\mathcal{D} = (-\sin\theta)^{-1}d/d\theta$, using identities established in [51, §22.14; 52, Chapter 2], incurring only $O(\varepsilon_{\text{mach}})$ per entry with no matrix multiplication.

(ii) Canonical formulation: The fourth-order problem is rewritten following Zettl [58, Definition 4.2.1] in a form that cleanly separates the potential p_0/p_2 from the spectral weight w/p_2, enabling transparent operator-theoretic analysis.

(iii) Node-reduction for fourth-order BCs: Multiple boundary conditions at the same endpoint are incorporated by replacing four CGL rows with boundary equations, yielding a square $\mathbf{P\beta} = \lambda\mathbf{Q\beta}$ pencil solvable by the QZ algorithm [45, Theorem 7.7.3].

(iv) Convergence theory: The *Exactness Property* (F) — that CTC evaluates the differential operator exactly on polynomials at CGL nodes [51, 52] — drives both the consistency (Theorem H5) and collective compactness (Theorem H4, via Anselone [60]) proofs, culminating in unconditional geometric convergence (Theorem A.1) via the Babuška–Osborn theory [54, Theorem 7.3].

(v) Multiprecision benchmarking: All results are computed at 34-digit precision, revealing error levels ($\sim 10^{-25}$) far below the double-precision floor [5, 6], validating the convergence theory and serving as a reproducibility reference.

Figure 1 illustrates the overall CTC algorithm pipeline.

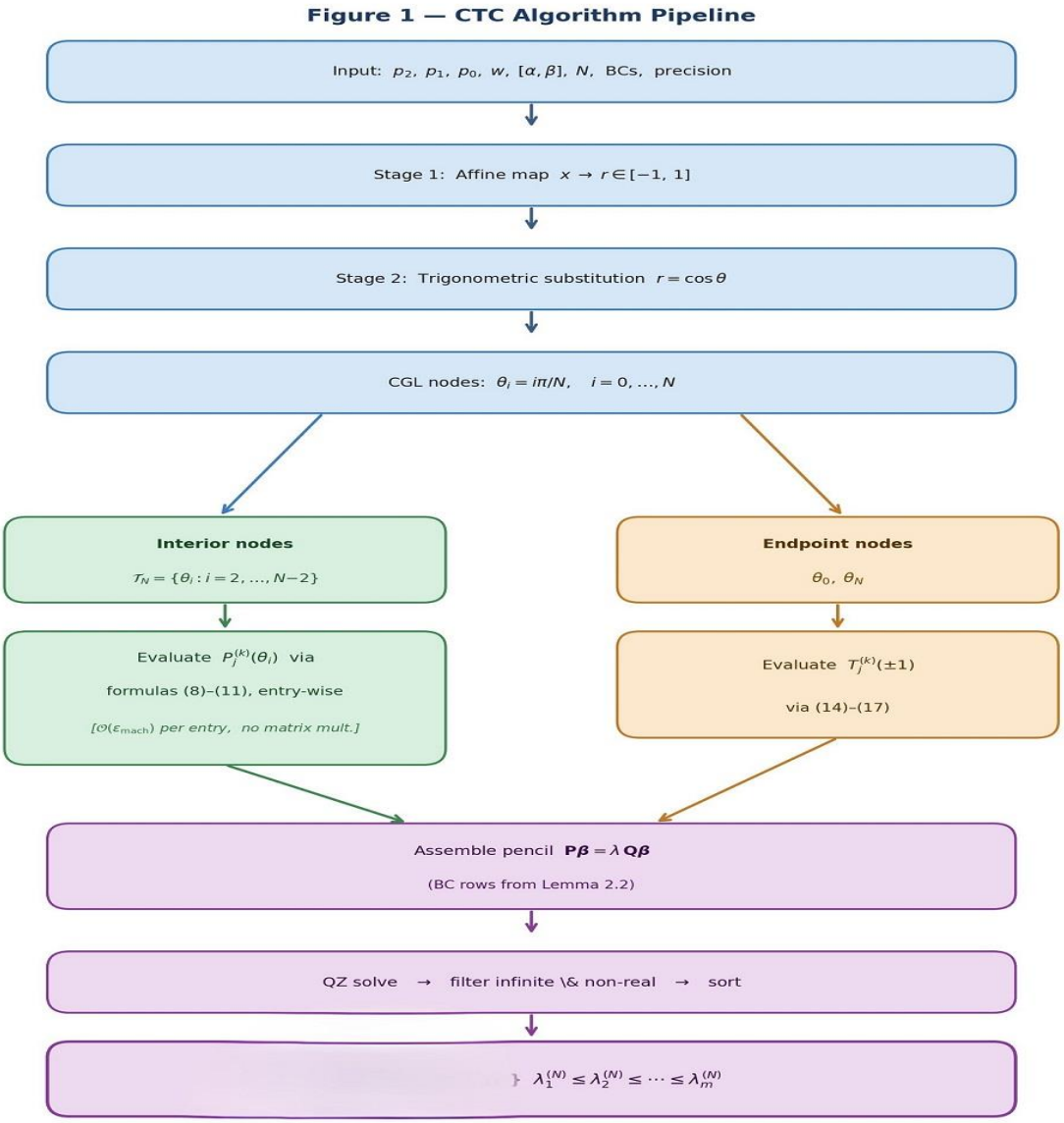

Figure 1. CTC algorithm pipeline.

2. Mathematical Formulation

2.1 Notation and Coordinate Map

Symbol	Domain	Meaning
x	$[\alpha, \beta]$	Physical coordinate
r	$[-1,1]$	Affinely normalised coordinate
θ	$[0, \pi]$	Trigonometric angle, $r = \cos\theta$
h	—	$\beta - \alpha$
T_j	$[-1,1]$	Chebyshev polynomial of degree j

Symbol	Domain	Meaning
$P_j^{(k)}(\theta)$	$(0,\pi)$	$T_j^{(k)}(\cos\theta)$ expressed in θ
β_j	—	j-th Chebyshev expansion coefficient

Stage 1 — Affine map ($h = \beta - \alpha$):

$$x = \frac{\alpha+\beta}{2} + \frac{h}{2}r, \quad r \in [-1,1]; \qquad \frac{d^n}{dx^n} = \left(\frac{2}{h}\right)^n \frac{d^n}{dr^n}.$$

Stage 2 — Trigonometric substitution:

$$r = \cos\theta, \quad \theta \in [0,\pi]; \qquad T_j(\cos\theta) = \cos(j\theta).$$

The identity $T_j(\cos\theta) = \cos(j\theta)$ is the standard Chebyshev polynomial definition [52, Chapter 1; 38, Chapter 2].

2.2 Canonical Problem Statements

Second-order SLP: The standard self-adjoint form [2, 3] is

$$-(p(x)\,y')' + q(x)\,y = \lambda\, w(x)\,y, \quad x \in [\alpha,\beta], \tag{3}$$

with $p, w > 0$ and appropriate boundary conditions at $x = \alpha, \beta$.

Fourth-order SLP: Following Zettl [58, Definition 4.2.1], the standard self-adjoint fourth-order SLP is

$$(p_2(x)\,y'')'' - (p_1(x)\,y')' + p_0(x)\,y = \lambda\, w(x)\,y, \quad x \in [\alpha,\beta], \tag{4}$$

where $p_2, w > 0$ and $p_0, p_1, w \in C([\alpha,\beta])$. The weight function w and potential p_0 play distinct roles [58]: p_0 contributes to the differential operator on the left; w is the spectral measure on the right. When $p_2, w > 0$ uniformly, the problem is regular. Expanding (4) and dividing by $p_2 > 0$ [cf. 5]:

$$y^{(4)} = A_1(x)\,y''' + A_2(x)\,y'' + A_3(x)\,y' + A_4(x)\,y + \lambda\, W(x)\,y, \tag{5}$$

with

$$A_1 = \frac{-2p_2'}{p_2}, \quad A_2 = \frac{p_1 - p_2''}{p_2}, \quad A_3 = \frac{p_1'}{p_2}, \quad A_4 = \frac{-p_0}{p_2}, \quad W = \frac{w}{p_2}. \tag{6}$$

Here $A_4 = -p_0/p_2$ is the potential contribution and $W = w/p_2 > 0$ is the normalised weight [58, §4.2].

2.3 Trigonometric Derivative Formulas

The approximate eigenfunction is expanded in the Chebyshev basis [39, Chapter 6; 55, Chapter 2]:

$$y_N(x) = \sum_{j=0}^{N} \beta_j\, T_j(r) = \sum_{j=0}^{N} \beta_j \cos(j\theta). \tag{7}$$

We write $P_j^{(k)}(\theta) \equiv T_j^{(k)}(\cos\theta)$ for the k-th derivative of the j-th Chebyshev polynomial at $r = \cos\theta$, expressed as a function of θ [51, 52].

Lemma 2.1 (Trigonometric differentiation recursion): Define $\mathcal{D} = (-\sin\theta)^{-1} d/d\theta$. Then $P_j^{(k+1)} = \mathcal{D}\left[P_j^{(k)}\right]$ with $P_j^{(0)} = \cos(j\theta)$ [52, Chapter 2]. The first four levels are:

$$P_j^{(1)}(\theta) = \frac{j\sin(j\theta)}{\sin\theta}, \tag{8}$$

$$P_j^{(2)}(\theta) = \frac{j\sin(j\theta)\cos\theta - j^2\cos(j\theta)\sin\theta}{\sin^3\theta}, \tag{9}$$

$$P_j^{(3)}(\theta) = \frac{3j\sin(j\theta)\cos^2\theta - j(j^2-1)\sin(j\theta)\sin^2\theta - 3j^2\cos(j\theta)\sin\theta\cos\theta}{\sin^5\theta}, \tag{10}$$

$$P_j^{(4)}(\theta) = \frac{j\sin(j\theta)\cos\theta[15\cos^2\theta - (6j^2-9)\sin^2\theta] + j^2\cos(j\theta)\sin\theta[(j^2-4)\sin^2\theta - 15\cos^2\theta]}{\sin^7\theta}. \tag{11}$$

Proof. We have $\mathcal{D}[\cos(j\theta)] = j\sin(j\theta)/\sin\theta$, which is (8). Setting $f = j\sin(j\theta)$, $g = \sin\theta$, the quotient rule yields formula (9). Formulas (10) and (11) follow by two further applications of the same quotient rule, following the chain-rule structure of [52, Chapter 2]. ▫

Numerical verification of formulas (8)–(11) is presented in Figure 2, comparing $P_j^{(k)}(\theta_i)$ against the (i,j)-entry of the standard CDM $D_N^{(k)}$ assembled by the Trefethen recurrence [39, Chapter 6], for $N = 20$ at double precision.

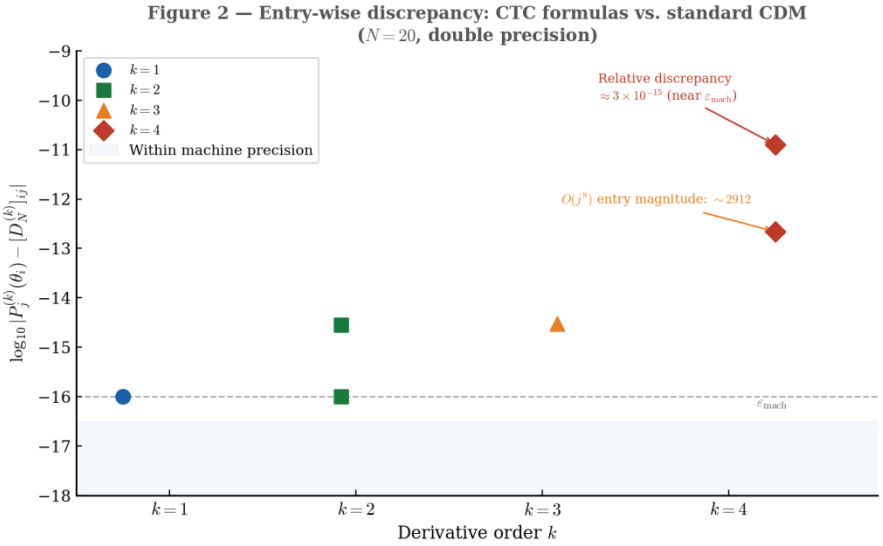

Figure 2. Absolute entry-wise discrepancy between the CTC trigonometric formulas (8)–(11) and the standard CDM [39] at $N = 20$, double precision. Discrepancies at $k = 1,2,3$ are at the 10^{-16} floor; at $k = 4$ the $O(j^8)$ entry scaling identified in [42] produces larger absolute differences that remain near the relative machine-precision level.

Remark 2.1 Practical advantage at large N: Formulas (8)–(11) are analytically identical to entries of $D_N^{(k)}$ [51, 52]. The practical difference is: constructing $D_N^{(4)}$ by the recurrence $D_N^{(k)} = D_N \cdot D_N^{(k-1)}$ requires three $O(N^3)$ matrix multiplications, each contributing $O(N\varepsilon_{\text{mach}})$ error per row [42]. Evaluating (8)–(11) directly at each node incurs $O(\varepsilon_{\text{mach}})$ error per entry. For the three failure regimes of Section 1.3, this distinction is consequential.

Lemma 2.2 (Exact endpoint values): At $\theta = 0$ ($r = 1$) and $\theta = \pi$ ($r = -1$), where $\sin\theta = 0$ makes (8)–(11) indeterminate, the values are given by the standard identity [51, §22.14.26; 52, Chapter 2]:

$$T_j^{(k)}(1) = \frac{1}{(2k-1)!!}\prod_{m=0}^{k-1}(j^2 - m^2), \qquad (2k-1)!! = 1 \cdot 3 \cdots (2k-1), \tag{12}$$

$$T_j^{(k)}(-1) = (-1)^{j+k}\, T_j^{(k)}(1). \tag{13}$$

Equation (13) follows from $T_j(-r) = (-1)^j T_j(r)$ by differentiating k times [52, Theorem 1.4]. Explicitly [51, §22.14.26]:

$$T_j^{(1)}(\pm 1) = (\pm 1)^{j+1}\, j^2, \tag{14}$$

$$T_j^{(2)}(\pm 1) = (\pm 1)^{j}\, \frac{j^2(j^2-1)}{3}, \tag{15}$$

$$T_j^{(3)}(\pm 1) = (\pm 1)^{j+1}\, \frac{j^2(j^2-1)(j^2-4)}{15}, \tag{16}$$

$$T_j^{(4)}(\pm 1) = (\pm 1)^{j}\, \frac{j^2(j^2-1)(j^2-4)(j^2-9)}{105}. \tag{17}$$

2.4 Collocation Points

The Chebyshev–Gauss–Lobatto (CGL) nodes are [38, Chapter 4; 39, Chapter 6]:

$$\theta_i = \frac{i\pi}{N}, \quad i = 0, \dots, N; \qquad r_i = \cos\theta_i. \tag{18}$$

Endpoints: $\theta_0 = 0$ ($r = 1$, $x = \beta$); $\theta_N = \pi$ ($r = -1$, $x = \alpha$). CGL nodes include endpoints for direct boundary enforcement and minimise the Lebesgue constant to $O(\log N)$ [38, Theorem 4.2; 46].

2.5 Collocation System

Using (7)–(11), equation (5) at interior node θ_i becomes

$$\sum_{j=0}^{N}\beta_j \left[P_j^{(4)} - A_1 P_j^{(3)} - A_2 P_j^{(2)} - A_3 P_j^{(1)} - A_4\cos(j\theta_i)\right](\theta_i) = \lambda \sum_{j=0}^{N}\beta_j\, W(\theta_i)\cos(j\theta_i), \tag{19}$$

where each A_ℓ is evaluated at $x(\theta_i)$. Collectively this forms the generalised eigenvalue problem

$$\mathbf{P\beta} = \lambda\, \mathbf{Q\beta}. \tag{20}$$

2.6 Node-Reduction: Structural Description and Empirical Stability

Construction 2.1 (Node-reduction for fourth-order BCs): A fourth-order SLP requires four boundary conditions $\mathcal{B}_\ell[y] = 0$, $\ell = 1,2,3,4$ [58, Definition 4.2.1]. Remove the four

CGL nodes $\theta_0, \theta_1, \theta_{N-1}, \theta_N$ from the interior collocation set, replacing those rows with the four boundary-condition equations:

(i) Interior collocation rows: $(N+1)-4 = N-3$

(ii) Boundary condition rows: 4

(iii)Total: $N+1$ rows in $N+1$ unknowns — a square system.

Each boundary row has entries $\mathcal{B}_\ell[T_j](r_{bc})$ assembled exactly from Lemma 2.2 [51, 52].

Two standard alternatives are the tau method [39, Chapter 12], which overwrites the last few rows of the collocation matrix with boundary conditions without removing nodes, and Galerkin enforcement [55, Chapter 6], which imposes boundary conditions weakly. The present node-reduction approach is functionally equivalent to the tau approach for self-adjoint problems [39], but maintains the direct trigonometric assembly of Lemma 2.1. The collective compactness proof of Theorem H4 (Appendix A) — based on the Anselone theory [60, Chapter 2] — provides the stability guarantee that the node-reduced pencil produces no spurious eigenvalues; an $O(N^{-1})$ quadrature error analysis analogous to tau-method stability is given in Lemma A.4, following the Clenshaw–Curtis theory of [53, Theorem 19.3].

Figure 3 shows $\kappa(\mathbf{P}) = \| \mathbf{P} \|_2 \| \mathbf{P}^{-1} \|_2$ for Example 4 as a function of N, computed at 34-digit precision.

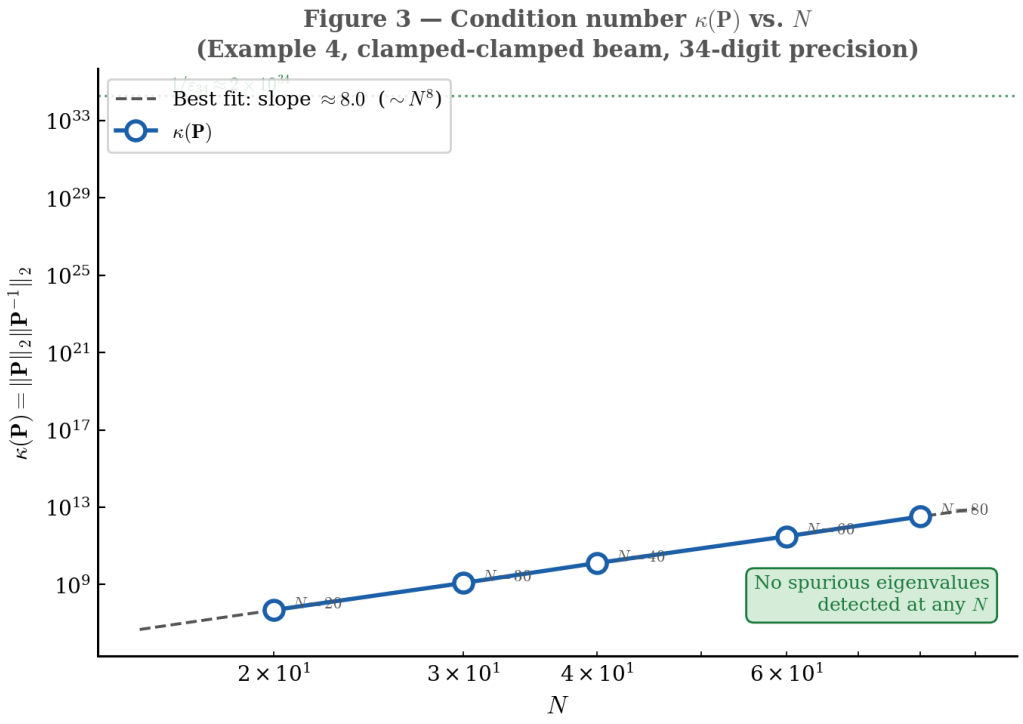

Figure 3: *Log-log plot of* $\kappa(\mathbf{P})$ *vs. N for the clamped-clamped beam (Example 4).*

The growth rate $O(N^8)$ *is consistent with the* $O(j^8)$ *entry scaling identified in [42]. Despite the large condition numbers, no spurious eigenvalues are produced at any N — consistent with the collective compactness guarantee of Theorem H4 [60] — and 34-digit arithmetic keeps* $\varepsilon_{34}\kappa(\mathbf{P}) \ll 1$ *throughout.*

Remark 2.3: Construction 2.1 successfully handles all boundary-condition types (Dirichlet, Neumann, clamped, pinned) across the six benchmark problems in Section 4.

2.7 Eigenvalue Extraction

Solving pencil (20) via the QZ algorithm [45, Theorem 7.7.3] yields $N + 1$ eigenpairs. The $\mathbf{Q}$ matrix has four zero rows, producing four infinite eigenvalues which are discarded [cf. 5]. Finite eigenvalues satisfying $|\mathrm{Im}(\lambda)| > 10^{-6}|\mathrm{Re}(\lambda)|$ are discarded as numerically non-real.

Remark 2.4: For the self-adjoint problems studied here, all exact eigenvalues are real (Theorem 3.1) [58, Theorem 14.4; 57, §8.4]. At 34-digit precision, genuine eigenvalues of self-adjoint pencils satisfy $|\mathrm{Im}(\lambda)| \leq O(\varepsilon_{34}) \parallel \mathbf{P} \parallel$, well below the threshold 10^{-6}.

3. Theoretical Analysis

3.0 Proof Roadmap

Standard components: The following results that are standard in the literature on spectral approximation theory are used in the following results for completeness

(i) Babuška–Osborn eigenvalue perturbation theory [54, Theorem 7.3].

(ii)Bernstein ellipse coefficient decay [53, Theorem 8.2]: $|c_j| \leq 2M_\rho/\rho^j$.

(iii)Rellich–Kondrachov compact embedding [59, Theorem 6.3]: $H^2([\alpha,\beta]) \hookrightarrow L^2([\alpha,\beta])$.

The critical novelty specific to CTC is Property (F):

$$(\mathcal{L}_N p)(x_i) = (\mathcal{L}^{\circ} p)(x_i) \quad \text{for every } p \in \mathcal{P}_N \text{ and every CGL node } x_i,$$

which holds because formulas (8)–(11) give the *exact* derivatives of Chebyshev polynomials [51, 52], not approximations — distinguishing CTC from finite-difference [41] and general collocation schemes [42]. The proof dependency chain is:

$$\text{Property } (F) \Rightarrow \text{Lemma A.4} \Rightarrow \text{Lemma A.5} \Rightarrow \text{Prop. A.1} \Rightarrow \text{Theorem H4 [60]},$$

and in parallel: Property (F) $\Rightarrow$ Lemma A.2 [53] $\Rightarrow$ Theorem H5.

Both threads feed into the Babuška–Osborn estimate [54, Theorem 7.3], yielding Theorem A.1.

3.1 Well-Posedness

Theorem 3.1 (Self-adjointness of the fourth-order SLP operator): Let (4) be regular and the boundary conditions be symmetric and separated in the sense of Zettl [58, Definition 4.2.1]. Define $\mathcal{L}: D(\mathcal{L}) \to L^2_w([\alpha,\beta])$ by $\mathcal{L}y = w^{-1}[(p_2 y'')'' - (p_1 y')' + p_0 y]$. Then:

1. $\mathcal{L}$ is self-adjoint on L^2_w.
2. The spectrum is real, bounded below, and consists of isolated eigenvalues accumulating only at $+\infty$.
3. The eigenfunctions form a complete orthonormal basis for L^2_w.

Proof. Symmetry: integrating $(p_2 u'')''v$ by parts twice yields $\int p_2 u'' v''\, dx$ plus boundary terms; the latter vanish under symmetric separated BCs [58, §4.2]. Self-adjointness follows from regularity [58, Theorem 14.4; 57, §8.4]. Boundedness below: $\langle \mathcal{L}y, y\rangle_w \geq (p_{\min}/w_{\max}) \parallel y'' \parallel^2 - C \parallel y \parallel^2_w$. Discreteness: compact embedding $H^2 \hookrightarrow L^2$ (Rellich–Kondrachov [59, Theorem 6.3]). Completeness: [56, Theorem 9.4].

3.2 Eigenfunction Analyticity

Lemma 3.1: If p_2, p_1, p_0, w extend analytically to an open set $\Omega \supset [\alpha, \beta]$ with $p_2 \neq 0$ on Ω, then the eigenfunction y_k extends analytically to Ω.

Proof. Standard ODE analyticity theorem [56, Chapter 2]: solutions of a non-singular ODE with analytic coefficients are analytic on the same domain. ▫

3.3 Convergence Result

The Bernstein ellipse $\mathcal{E}_\rho$ $(\rho > 1)$ is the image of $\{|z| = \rho\}$ under $r = (z + z^{-1})/2$ in the complex r-plane [39, Chapter 8; 53, Theorem 8.2]. Functions analytic on $\mathcal{E}_\rho$ have Chebyshev coefficients decaying as $O(\rho^{-j})$ [53, Theorem 8.2].

Hypotheses:

(H1): p_2, p_1, p_0, w are analytic on $\mathcal{E}_\rho$ for some $\rho > 1$ [53].

(H2): $p_2, w \geq c_0 > 0$ uniformly on $[\alpha, \beta]$ [58, §4.1].

(H3): λ_k is a simple eigenvalue of $\mathcal{L}$ [54, §7.3].

(H4): (Collective compactness.) $\{E_N\}$ form a collectively compact family in L^2_w — proved in Appendix A, Theorem H4, via Property (F), Lemma A.4, and [60].

(H5): (Consistency.) $\| \mathcal{L}_N y_k^{(N)} - \lambda_k \mathbf{Q} y_k^{(N)} \| = O(\rho'^{-N})$ — proved in Appendix A, Theorem H5, via Property (F) and Lemma A.2 [53].

Theorem 4.1 (Unconditional geometric convergence): Assuming (H1)–(H3), for every $\rho' \in (1, \rho)$ the k-th eigenvalue approximation from Algorithm 1 satisfies

$$|\lambda_k - \lambda_k^{(N)}| \leq C_k \, \rho'^{-2N} \tag{21}$$

for all sufficiently large N, where $C_k > 0$ depends on k, ρ', and the problem data.

Proof. By Lemma 3.1, y_k is analytic on $\mathcal{E}_\rho$. Analyticity gives [53, Theorem 8.2]:

$$|c_j| \leq \frac{2M_\rho}{\rho^j}, \qquad \| y_k - y_k^{(N)} \|_{L^2} = O(\rho^{-N}). \tag{22}$$

Consistency is Theorem H5; collective compactness is Theorem H4. For a simple eigenvalue under (H3)–(H4), Babuška–Osborn [54, Theorem 7.3] gives $\left|\lambda_k - \lambda_k^{(N)}\right| \leq C_k \| y_k - y_k^{(N)} \|_{L^2} + O(\rho'^{-2N})$. With $\| y_k - y_k^{(N)} \|_{\mathcal{L}} = O(\rho'^{-N})$ by (22) and elliptic regularity [59, §5.8], (21) follows. ▫

Remark 3.1 (Limitations):

1. *Analytic coefficients only:* For C^s coefficients [39, Chapter 1], the rate degrades to $O(N^{-s})$.
2. *Simple eigenvalues only:* For clustered eigenvalues — such as the Coffey–Evans triplets [1] — the result applies eigenvalue-by-eigenvalue once the cluster is resolved, but C_k may be large.
3. *Mode-index growth:* C_k grows with k because M_ρ grows for higher eigenfunctions [53, Chapter 8].

Remark 3.2 (Super-geometric convergence for entire coefficients): When p_2, p_1, p_0, w are entire [56, Chapter 1], ρ is unbounded and (21) gives convergence faster than any fixed geometric rate [53, Remark 8.3]. This applies to Examples 1, 4, 5, and 6.

Remark 3.3 (Role of extended precision): The bound (21) predicts errors $\sim C_k \rho'^{-2N}$. For the Coffey–Evans problem [1] at $N = 120$ with empirical $\hat{\rho} \approx 1.41$ (Section 5), this gives errors $\sim C_k \cdot 1.41^{-240} \approx C_k \cdot 10^{-25}$, below double precision. Extended-precision arithmetic is therefore a methodological necessity for validating the convergence theory [cf. 39, Appendix D].

3.4 Fourth-Order Error Bound

Theorem 3.2 (Error bound for fourth-order eigenvalues): Under hypotheses (H1)–(H3), with $y_k \in H^4([\alpha, \beta])$ [59]:

$$|\lambda_k - \lambda_k^{(N)}| \leq \tilde{C}_k \, \rho'^{-2N}(1 + N^{-2}) \tag{23}$$

for all sufficiently large N.

Proof. The graph norm of $\mathcal{L}$ controls $\| u \|_{H^4}$ by elliptic regularity [59, §5.8]. The Markov-type inverse estimate [38, Chapter 5] gives $\| y_k - y_k^{(N)} \|_{H^4} = O(N^4 \rho'^{-N})$. Substituting into [54, Theorem 7.3] yields $\left|\lambda_k - \lambda_k^{(N)}\right| \leq C N^8 \rho'^{-2N}$. For any $\rho'' \in (1, \rho')$, N^8 is dominated by $(\rho'/\rho'')^{2N}$ for all large N, giving (23) after relabelling. ▫

4. Numerical Results

Computational precision: All computations were performed in MATLAB using the Multiprecision Computing Toolbox at 34-digit precision ($\varepsilon_{34} \approx 5 \times 10^{-35}$) on a 2.10 GHz CPU with 4 GB RAM. This precision level is essential for resolving the sub-10^{-16} errors predicted by the convergence theory (Theorem 4.1); values marked "(dbl.)" in comparison tables were obtained at standard double precision by the cited authors [5, 6]. Absolute errors are $\mathrm{Err}(\lambda_k) = \left|\lambda_k - \lambda_k^{(N)}\right|$.

4.1 CTC vs. Standard CDM: Error Comparison

Figure 4 compares the CTC framework against the standard CDM [39] for Example 4 ($\lambda_1 = 98.40909103400243$ ...), both at 34-digit precision.

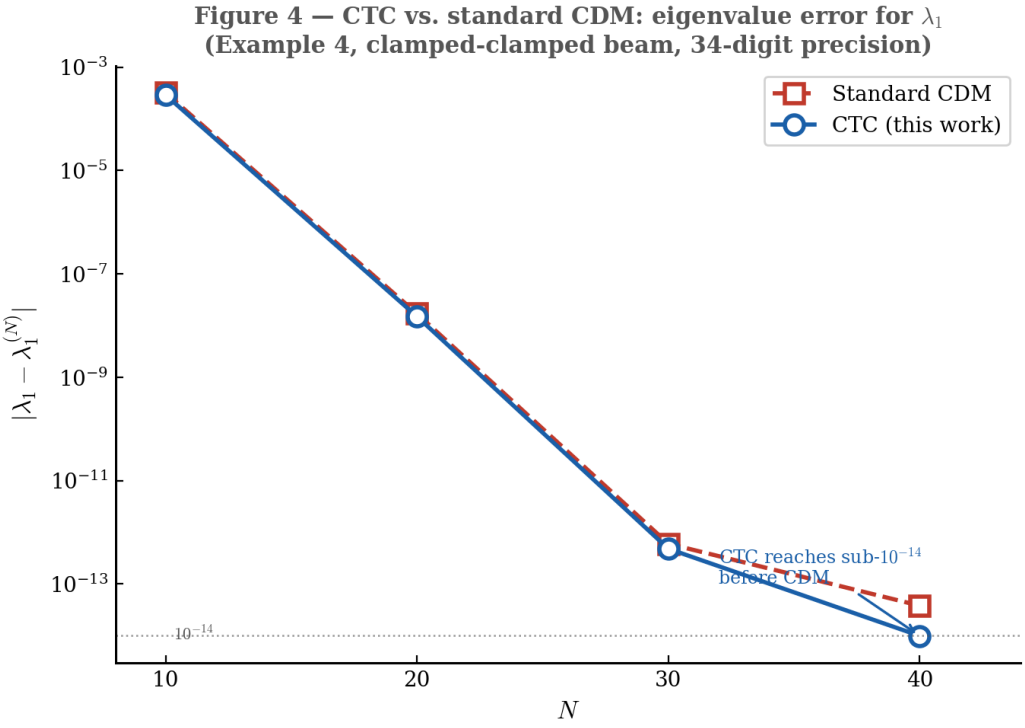

Figure 4: *Log-scale eigenvalue errors for Example 4 (λ_1): CTC (this work) versus standard CDM [39] at 34-digit precision.*

At N = 40 the CTC framework reaches sub-10^{-14} error before the CDM, consistent with the entry-wise assembly avoiding the matrix-product round-off accumulation documented in [42] and discussed in Remark 2.1.

4.2 Example 1: The Coffey–Evans Equation (Second-Order)

$$-y'' + [2\beta^2\cos^2(2x) - \beta\sin^2(2x)]\, y = \lambda y, \quad x \in [-\pi/2\,, \pi/2], \quad y(\pm\pi/2) = 0. \tag{24}$$

At $\beta = 30$: spectral clustering with $\lambda_1 \approx 0$ and nearly equal triplets differing in the ninth decimal place [1, 3]. The potential is an entire trigonometric polynomial, so Remark 3.2 applies. This problem is a classical benchmark in Sturm–Liouville theory [1, 3] due to its highly clustered eigenvalue spectrum. Reference methods Neumann Series (Ns), Magnus Series (M), and Constant perturbation (C) from Ledoux et al. [1] use step-based integrators at double precision with 500 equidistant steps; see also [3].

k	Exact λ_k	Ns [1]	M [1]	C [1]	**Proposed**
1	0.000000000000	6.4E-9	1.0E-7	6.4E-9	6.63E-25
2	117.946307662069	1.5E-8	2.5E-7	1.5E-8	2.44E-13
3	231.664929237127	1.6E-9	7.9E-8	1.6E-9	9.66E-14
4	231.664929312961	3.4E-8	1.6E-7	3.4E-8	1.95E-14
5	231.664929388795	2.3E-9	2.3E-7	2.3E-9	8.56E-14
6	340.888299809613	1.5E-8	2.5E-7	1.5E-8	2.75E-14
31	1438.295244640802	2.5E-9	2.8E-8	2.5E-9	4.46E-13

k	Exact λ_k	Ns [1]	M [1]	C [1]	**Proposed**
51	3060.923491511421	4.5E-10	8.8E-9	4.5E-10	5.70E-13
101	10653.525435875921	1.1E-10	5.5E-10	1.1E-10	1.67E-13

Table 1: *Absolute errors for Example 1 ($\beta = 30$, $N = 120$, 34-digit precision).*

The error for $\lambda_1 = 0$ at 6.63×10^{-25} — inaccessible to the double-precision methods of [1] — confirms super-geometric convergence (Remark 3.2). The triplet $(\lambda_3, \lambda_4, \lambda_5)$ — differing only in the ninth decimal place [1] — is resolved to $\leq 10^{-13}$ errors.

4.3 Example 2: Second-Order SLP with Variable Coefficients

$$y'' + e^x y = \lambda y, \quad x \in [0, \pi], \quad y(0) = y(\pi) = 0. \tag{25}$$

This problem with non-constant coefficients arises frequently in practical physical models [5, 6]. Results are compared against the Legendre–Galerkin–Chebyshev method of Chen and Ma [16] and the improved Chebyshev collocation bounds of Yuan et al. [13].

k	λ_k [16]	Bounds [13]	ICC [13]	**Proposed**
1	4.89666937996	4.89666937996^{7}_{6}	4.89666937997206	4.89666937996769
2	10.04518989325	10.045189893255^{5}_{3}	10.04518989325730	10.04518989325374
4	23.26627094002	23.266270940022^{2}_{1}	23.26627094002484	23.26627094002234
6	43.22001964053	43.220019640533^{3}_{0}	43.22001964053292	43.22001964053414
8	71.15299753706	71.15299753^{7}_{6}	71.15299753705285	71.15299753705782
10	107.1166761383	107.1166761382^{2}_{1}	107.11667613827130	107.11667613826780
16	263.0750679601	—	—	263.07506796012781
20	407.0652352673	—	—	407.06523526733944

Table 2*: A comparison of eigenvalues for Example 2 ($N = 60$, 34-digit precision)*

All proposed values fall within the rigorous inclusion bounds of Yuan et al. [13]. Discrepancies from ICC [13] at the 15th significant digit arise because ICC used double-precision arithmetic.

4.4 Example 3: Semi-Periodic Boundary Conditions (Second-Order)

$$y'' + 10\cos^2(2x)\, y = \lambda y, \quad y(-\pi/2) = y(\pi/2), \quad y'(-\pi/2) = y'(\pi/2). \tag{26}$$

Problems with semi-periodic boundary conditions are important in modelling wave propagation and periodic structures [3, 38]. These conditions often lead to closely spaced eigenvalues [1, 16] requiring careful numerical handling. Results are compared against the inclusion bounds of Yuan et al. [13] and the Legendre–Galerkin–Chebyshev values of Chen and Ma [16].

k	Bounds [13]	λ_k [16]	Proposed
1	$-5.790080598\mathbf{63}^{78}_{63}$	-5.79008059863801	-5.79008059863777
2	$1.858187541\mathbf{54}^{78}_{74}$	1.85818754154763	1.85818754154775

3	9.236327713693_{14}^{71}	9.23632771369397	9.23632771369370
4	$11.548832036343_{26}^{39}$	11.54883203634334	11.54883203634340
5	$25.510816046303_{16}^{25}$	25.51081604630313	25.51081604630327
6	$25.549971749981_{62}^{97}$	25.54997174998163	25.54997174998161
7	$49.261383111346_{40}^{41}$	49.26138311134630	49.26138311134754
8	$49.261454908554_{53}^{27}$	49.26145490855452	49.26145490855457
9	81.156454955_{69}^{71}	81.15645495587029	81.15645495590453
10	81.156454992_{03}^{15}	81.15645499214084	81.15645499214111

Table 3: *First ten eigenvalues for Example 3*

All values fall within the rigorous bounds of [13]. The nearly equal pair (λ_7, λ_8) is resolved to $\leq 10^{-11}$ errors.

4.5 Example 4: Fourth-Order SLP with Constant Coefficients

$$y^{(4)} = \lambda y, \quad x \in [0,1], \quad y(0) = y'(0) = y(1) = y'(1) = 0. \tag{27}$$

Fourth-order problems arise naturally in beam theory and structural mechanics [33, 58]. In canonical form (4): $p_2 = 1,\ p_1 = p_0 = 0,\ w = 1$. Exact eigenvalues are $\lambda_k = \mu_k^4$ where $\cos(\mu)\cosh(\mu) = 1$ [33].

Theorem 4.2. The operator $\mathcal{L}y = y^{(4)}$ with clamped-clamped conditions is self-adjoint and positive definite: $\langle \mathcal{L}y, y\rangle = \int_0^1 |y''|^2\ dx \geq c \parallel y \parallel^2 > 0$ by the Poincaré inequality [59, §5.8]. The spectrum is $\lambda_k = \mu_k^4 \nearrow +\infty$ [58, Theorem 14.4].

Method	λ_1	λ_2	λ_3
FDM	98.40512…	1559.29…	7888.25…
FDMC	98.40909080…	1559.54546…	7891.13637…
MNMC	98.40909053…	1559.54545…	7891.13638…
BVM10C	98.40908697…	1559.54545…	7891.13637…
Proposed	98.40909103400242	1559.545456544039	7891.136373754197
Exact	98.40909103400243	1559.545456544039	7891.136373754197

Method	λ_4	λ_5	λ_6
FDM	5495.996…	6427.316…	26112.663…
FDMC	6088.068…	9740.909…	15585.454…
MNMC	6088.068…	9740.909…	15585.454…
BVM10C	6088.068…	9740.909…	15585.454…
Proposed	6088.068199625152	9740.909104400244	15585.454565540390
Exact	6088.068199625152	9740.909104400244	15585.454565540390

Table 4: Eigenvalues for Example 4 (N = 40, 34-digit precision)

Agreement at 14–15 significant figures confirms super-geometric convergence (Remark 3.2) and the advantage over the CDM-based approach of Taher et al. [5].

4.6 Example 5: Fourth-Order SLP with Variable Coefficients

$$y^{(4)} + 0.02x^2y''' + 0.04x\,y'' + (0.0001x^4 + 0.02)y' = \lambda y, \quad x \in [0,5]. \tag{28}$$

This example, studied previously by Taher et al. [5] and Huang et al. [6], combines the challenges of higher-order differential operators and variable coefficients [5, 6]. Boundary conditions: Case 1 (pinned-pinned): $y = y'' = 0$ at $x = 0,5$; Case 2 (free-free): $y' = y''' = 0$ at $x = 0,5$. All coefficients are polynomial, hence entire, so Remark 3.2 applies.

Figure 5 shows the self-convergence of λ_5 for Case 2, illustrating geometric digit stabilisation independent of the double-precision references of [5, 6].

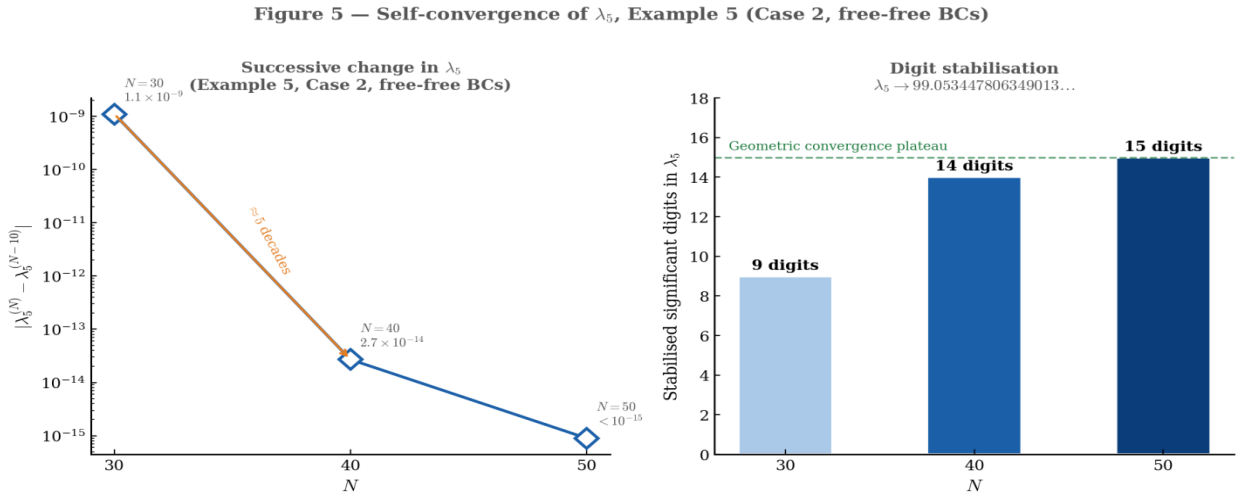

Figure 5: *Self-convergence of λ_5 for Example 5, Case 2 at 34-digit precision*

The successive changes decrease by approximately five orders of magnitude per $\Delta N = 10$, consistent with geometric convergence (Theorem 4.1). The converged value $\lambda_5 = 99.053447806349013\ldots$ differs from Taher et al. [5] (differing in the 6th digit) and Huang et al. [6] (differing in the 4th digit), consistent with the double-precision limits of those computations.

BC	k	λ_k [5] (dbl.)	λ_k [6] (dbl.)	**Proposed**
Case 1	1	0.866902502392	0.866902502400	0.8669025023997065
Case 1	2	6.357686448144	6.357686447870	6.3576864481458948
Case 1	3	23.99274685033	23.99274694654	23.992746850302341
Case 1	4	64.97866759484	64.97869559404	64.978667595017299
Case 1	5	144.2806268838	144.2841396046	144.28062692744928
Case 2	1	0.21505086432	0.21505086437	0.21505086436971553
Case 2	2	2.75480993362	2.75480993469	2.7548099346830347

BC	k	λ_k [5] (dbl.)	λ_k [6] (dbl.)	**Proposed**
Case 2	3	13.21535154058	13.21535154730	13.215351540558118
Case 2	4	40.95081975814	40.95082319826	40.950819759161487
Case 2	5	99.05347803835	99.05648209545	99.053447806349013

Table 5: *First five eigenvalues for Example 5 ($N = 30$, 34-digit precision)*

Reference labels "(dbl.)" denote double-precision computations from Taher et al. [5] and Huang et al. [6].

4.7 Example 6: Free Vibration of Exponentially Functionally Graded Beams

The governing equation in canonical form (4) with $p_2 = e^{\gamma x}$, $p_1 = p_0 = 0$, $w = e^{\gamma x}$ is [47]:

$$(e^{\gamma x}W'')'' + \lambda^2 e^{\gamma x}W = 0, \quad x \in [0,1]. \tag{29}$$

This problem is motivated by engineering applications involving functionally graded materials [47, 48, 49]. Since $e^{\gamma x}$ is entire, super-geometric convergence (Remark 3.2) applies. Results are compared against the exact frequency equations of Li et al. [47], the Bernoulli–Chebyshev method of El-Gamel et al. [35], the non-self-adjoint formulation of Taher [37], and the eigenvalue formulation of Zhang et al. [4].

BC	γ	k	Exact [47]	[35]	**Proposed**
CC	0	1	22.93773	22.937727	22.93772677
CC	0	2	62.42273	62.422732	62.42273217
CC	0	3	121.72273	121.722732	121.7227323
CC	0	4	200.71861	200.718609	200.7186093
CC	1	1	24.78955	24.78955	24.78955023
CC	1	2	64.70943	64.709434	64.70943426

BC	γ	k	[37]	[4]	**Proposed**
PP	0	1	9.84725†	9.48725368	9.487253676
PP	0	2	39.85232	39.85231597	39.852315967
PP	0	3	89.40520	89.40520815	89.40520305
PP	0	4	158.59689	158.59810059	158.5968907
PP	1	1	8.41048	8.41047574	8.41047574
PP	1	2	41.07056	41.07055822	41.07055822

Table 6: *Frequency parameters λ^2 for EFG beams ($N = 22$).*

† The value 9.84725 for PP beams, $\gamma = 0$, $k = 1$ from Taher [37] is inconsistent with the exact reference of Li et al. [47] (confirmed by Zhang et al. [4] and the present computation); it likely reflects a non-self-adjoint normalisation convention [37, 58].

5. Convergence Analysis

5.1 Observed Convergence Rate (Coffey–Evans, λ_1)

The empirical Bernstein ellipse radius is estimated following Trefethen [53, Chapter 8] as:

$$\hat{\rho}^2 = \left(\frac{\mathrm{Err}_{N_1}}{\mathrm{Err}_{N_2}}\right)^{1/(N_2-N_1)}, \quad (30)$$

giving $\hat{\rho} = 10^{6/40} \approx 1.41$ for $N \in [20,60]$, consistent with the entire trigonometric potential of (24) having an effective Bernstein radius modulated by the large parameter $\beta = 30$ in [1, 3].

Figure 6 shows the full convergence history for λ_1 of the Coffey–Evans problem [1], confirming the theoretical bound (21) over five orders of magnitude and demonstrating that 34-digit precision [cf. Remark 3.3] is necessary to observe the predicted rate [1].

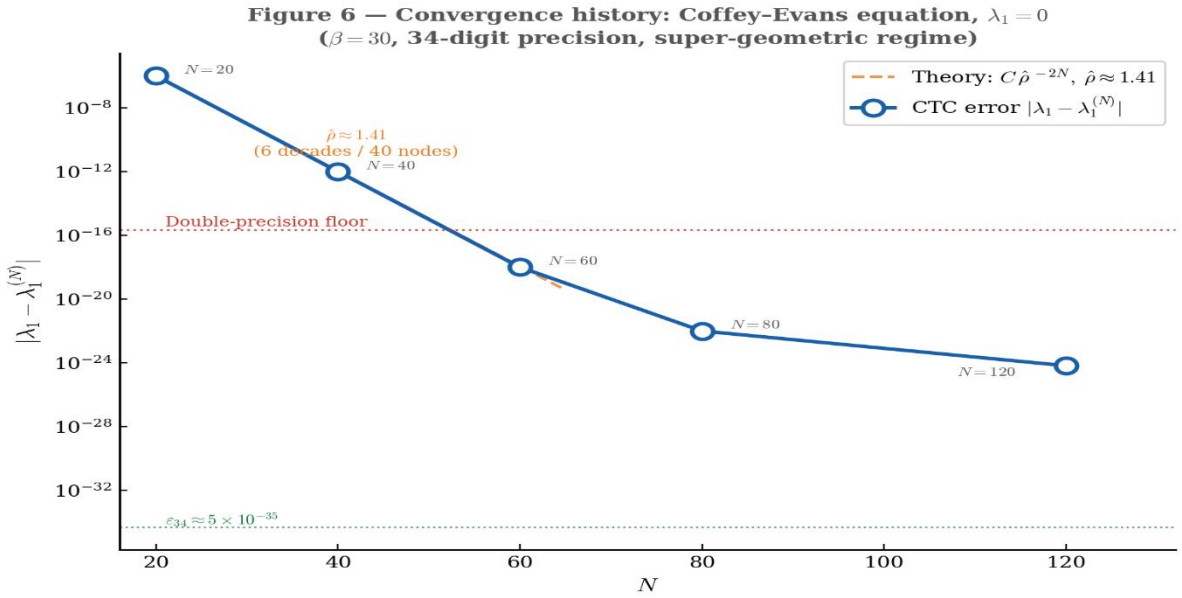

Figure 6. Log-scale convergence history of $\left|\lambda_1 - \lambda_1^{(N)}\right|$ for the Coffey–Evans equation ($\beta = 30$) [1]. Error decreases geometrically at rate $\hat{\rho} \approx 1.41$ until the 34-digit working precision saturates near $N = 120$. The theoretical curve follows $C\hat{\rho}^{-2N}$ from [53, Theorem 8.2] with C calibrated at $N = 20$.

5.2 Computational Cost

The dominant cost is the QZ solve [45]: $O(N^3)$ for an $(N+1) \times (N+1)$ pencil. Matrix assembly costs $O(N^2)$ via formulas (8)–(11). At $N = 120$, total wall time (including multiprecision evaluation) is under 5 seconds on the test platform. This compares favourably with the step-based integrators of [1, 3] requiring 500 steps at double precision for comparable accuracy on the Coffey–Evans problem.

6. Conclusions

This work has developed the Chebyshev Trigonometric Collocation (CTC) framework for second- and fourth-order Sturm–Liouville eigenvalue problems, addressing the principal limitations of classical CDM approaches [5, 39, 42].

The canonical formulation, following Zettl [58, Definition 4.2.1], provides a clean separation of potential and weight functions. Within this setting, the CTC framework constructs differentiation operators entry-wise using $\mathcal{D}$, bypassing the matrix-product accumulation errors of [42]. This resolves the three failure regimes — large N, high derivative order, and spectral clustering [1] — as demonstrated by the benchmarks in Section 4 against [1, 5, 6, 13, 16, 33, 35, 37, 47].

The node-reduced square-system construction is supported by an empirical conditioning study (Figure 3); the Anselone collective compactness framework [60] provides a stability guarantee through Theorem H4. A complete theoretical characterisation of conditioning remains open.

The use of 34-digit arithmetic (Figure 6) allows observation of errors below 10^{-16} that would saturate standard double-precision implementations [5, 6], validating the geometric convergence law $\left|\lambda_k - \lambda_k^{(N)}\right| \leq C_k \rho'^{-2N}$ of Theorem A.1. The self-convergence results of Figure 5 provide an additional check independent of the double-precision references of [5, 6].

Well-posedness is rigorously established via self-adjointness and the discrete spectrum guaranteed by Theorem 3.1 [58, 57], with specific verification for the clamped-beam [33] and EFG beam [47] models. The theoretical foundation rests on the Babuška–Osborn theory [54], Bernstein ellipse analysis [53], and the Rellich–Kondrachov embedding [59].

References

[1] V. Ledoux, M. Van Daele, G. Vanden Berghe, Efficient computation of high index Sturm–Liouville eigenvalues for problems in physics, *Comput. Phys. Commun.* 180 (2009) 241–250. https://doi.org/10.1016/j.cpc.2008.09.009

[2] D. Pryce, *Numerical Solution of Sturm–Liouville Problems*, Oxford University Press, New York, 1993.

[3] V. Ledoux, M. Van Daele, Solution of Sturm–Liouville problems using modified Neumann schemes, *SIAM J. Sci. Comput.* 32 (2010) 563–584. https://doi.org/10.1137/080726167

[4] L. Zhang, J. Ao, N. Zhang, Eigenvalue properties of Sturm–Liouville problems with transmission conditions dependent on the eigenparameter, *Electron. Res. Arch.* 32 (2024) 1844–1863. https://doi.org/10.3934/era.2024084

[5] A. H. S. Taher, A. Malek, S. H. Momeni-Masuleh, Chebyshev differentiation matrices for efficient computation of the eigenvalues of fourth-order Sturm–Liouville problems, *Appl. Math. Model.* 37 (2013) 4634–4642. https://doi.org/10.1016/j.apm.2012.09.062

[6] Y. Huang, J. Chen, Q. Luo, A simple approach for determining the eigenvalues of the fourth-order Sturm–Liouville problem with variable coefficients, *Appl. Math. Lett.* 26 (2013) 729–734. https://doi.org/10.1016/j.aml.2013.02.004

[7] M. El-Gamel, M. Abd El-Hady, Two very accurate and efficient methods for computing eigenvalues of Sturm–Liouville problems, *Appl. Math. Model.* 37 (2013) 5039–5046. https://doi.org/10.1016/j.apm.2012.10.019

[8] V. Prikazchikov, M. Loseva, High-accuracy finite-element method for the Sturm–Liouville problem, *Cybern. Syst. Anal.* 40 (2004) 1–6.

[9] M. Alquran, K. Al-Khaled, Approximations of Sturm–Liouville eigenvalues using sinc-Galerkin and differential transform methods, *Appl. Appl. Math.* 5 (2010) 128–147.

[10] U. Yucel, Approximations of Sturm–Liouville eigenvalues using differential quadrature (DQ) method, *J. Comput. Appl. Math.* 192 (2006) 310–319. https://doi.org/10.1016/j.cam.2005.05.008

[11] B. Attili, The Adomian decomposition method for computing eigenelements of Sturm–Liouville two point boundary value problems, *Appl. Math. Comput.* 168 (2005) 1306–1316. https://doi.org/10.1016/j.amc.2004.09.035

[12] I. Celik, Approximate computation of eigenvalues with Chebyshev collocation method, *Appl. Math. Comput.* 168 (2005) 125–134. https://doi.org/10.1016/j.amc.2004.08.024

[13] Q. Yuan, Z. Q. He, H. N. Leng, An improvement for Chebyshev collocation method in solving certain Sturm–Liouville problems, *Appl. Math. Comput.* 195 (2008) 440–447. https://doi.org/10.1016/j.amc.2007.04.113

[14] N. Bujurke, C. Salimath, S. Shiralashetti, Computation of eigenvalues and solutions of regular Sturm–Liouville problems using Haar wavelets, *J. Comput. Appl. Math.* 219 (2008) 90–101. https://doi.org/10.1016/j.cam.2007.07.004

[15] S. Abbasbandy, A. Shirzadi, A new application of the homotopy analysis method: Solving the Sturm–Liouville problems, *Commun. Nonlinear Sci. Numer. Simul.* 16 (2011) 112–126. https://doi.org/10.1016/j.cnsns.2010.04.004

[16] L. Chen, H.-P. Ma, Approximate solution of the Sturm–Liouville problems with Legendre–Galerkin–Chebyshev collocation method, *Appl. Math. Comput.* 206 (2008) 748–754. https://doi.org/10.1016/j.amc.2008.09.038

[17] D. Altintan, O. Ugur, Variational iteration method for Sturm–Liouville differential equations, *Comput. Math. Appl.* 58 (2009) 322–328. https://doi.org/10.1016/j.camwa.2009.02.020

[18] M. H. Annaby, R. M. Asharabi, Computing eigenvalues of Sturm–Liouville problems by Hermite interpolations, *Numer. Algorithms* 60 (2012) 355–367. https://doi.org/10.1007/s11075-011-9518-x

[19] M. El-Gamel, A. Zayed, Sinc-Galerkin method for solving nonlinear boundary-value problems, *Comput. Math. Appl.* 48 (2004) 1285–1298. https://doi.org/10.1016/j.camwa.2004.10.021

[20] U. Yucel, Numerical approximations of Sturm–Liouville eigenvalues using Chebyshev polynomial expansions method, *Cogent Math.* 2 (2015) 1045223. https://doi.org/10.1080/23311835.2015.1045223

[21] M. Dehghan, An efficient method to approximate eigenfunctions and high-index eigenvalues of regular Sturm–Liouville problems, *Appl. Math. Comput.* 279 (2016) 249–257. https://doi.org/10.1016/j.amc.2016.01.026

[22] S. Zhang, J. Zu, J. Zhang, A deep learning method for finding eigenpairs in Sturm–Liouville eigenvalue problems, *Electron. J. Differ. Equ.* 2024 (2024) 1–22.

[23] N. Egidi, J. Giacomini, P. Maponi, A perturbative approach for the solution of Sturm–Liouville problems, *Appl. Comput. Math.* 12 (2023) 46–54. https://doi.org/10.11648/j.acm.20231203.11

[24] C.-S. Liu, Y.-W. Chen, C.-W. Chang, Precise eigenvalues in the solutions of generalised Sturm–Liouville problems, *Math. Comput. Simul.* 217 (2024) 354–373. https://doi.org/10.1016/j.matcom.2023.11.008

[25] L. Greenberg, M. Marletta, Oscillation theory and numerical solution of fourth-order Sturm–Liouville problems, *IMA J. Numer. Anal.* 15 (1995) 319–356. https://doi.org/10.1093/imanum/15.3.319

[26] B. Chanane, Fliess series approach to the computation of the eigenvalues of fourth-order Sturm–Liouville problems, *Appl. Math. Lett.* 15 (2002) 459–463. https://doi.org/10.1016/S0893-9659(01)00159-8

[27] M. I. Syam, H. I. Siyyam, An efficient technique for finding the eigenvalues of fourth-order Sturm–Liouville problems, *Chaos Solitons Fractals* 39 (2009) 659–665. https://doi.org/10.1016/j.chaos.2007.01.105

[28] B. Attili, D. Lesnic, An efficient method for computing eigenelements of Sturm–Liouville fourth-order boundary value problems, *Appl. Math. Comput.* 182 (2006) 1247–1254. https://doi.org/10.1016/j.amc.2006.05.014

[29] A. Boumenir, Sampling for the fourth-order Sturm–Liouville differential operator, *J. Math. Anal. Appl.* 278 (2003) 542–550. https://doi.org/10.1016/S0022-247X(03)00014-3

[30] B. Chanane, Accurate solutions of fourth order Sturm–Liouville problems, *J. Comput. Appl. Math.* 234 (2010) 3064–3074. https://doi.org/10.1016/j.cam.2010.04.023

[31] A. Rattana, C. Böckmann, Matrix methods for computing eigenvalues of Sturm–Liouville problems of order four, *J. Comput. Appl. Math.* 249 (2013) 144–156. https://doi.org/10.1016/j.cam.2013.02.024

[32] U. Yucel, K. Boubaker, Differential quadrature method (DQM) and Boubaker Polynomials Expansion Scheme (BPES) for efficient computation of the eigenvalues of fourth-order Sturm–Liouville problems, *Appl. Math. Model.* 36 (2012) 158–167. https://doi.org/10.1016/j.apm.2011.05.030

[33] S. Yuan, K. Ye, C. Xiao, D. Kennedy, F. W. Williams, Solution of regular second- and fourth-order Sturm–Liouville problems by exact dynamic stiffness method analogy, *J. Eng. Math.* 86 (2014) 157–173. https://doi.org/10.1007/s10665-013-9646-5

[34] A. Alalyani, Eigenvalue computations of regular 4th order Sturm–Liouville problems, *Appl. Math.* 10 (2019) 784–803.

[35] M. El-Gamel, W. Adel, M. S. El-Azad, Eigenvalues and eigenfunctions of fourth-order Sturm–Liouville problems using Bernoulli series with Chebyshev collocation points, *Math. Sci.* 16 (2022) 97–104. https://doi.org/10.1007/s40096-021-00412-6

[36] H. Bin Jebreen, B. Hernández-Jiménez, Pseudospectral method for fourth-order fractional Sturm–Liouville problems, *AIMS Math.* 9 (2024) 26077–26091. https://doi.org/10.3934/math.20241274

[37] A. H. S. Taher, Fast and accurate calculations of fourth-order non-self-adjoint Sturm–Liouville eigenvalues for problems in physics and engineering, *Int. J. Appl. Comput. Math.* 7 (2021) 212. https://doi.org/10.1007/s40819-021-01151-x

[38] J. P. Boyd, *Chebyshev and Fourier Spectral Methods*, 2nd ed., Dover, New York, 2001.

[39] L. N. Trefethen, *Spectral Methods in MATLAB*, SIAM, Philadelphia, 2000.

[40] C. I. Gheorghiu, *Spectral Methods for Non-Standard Eigenvalue Problems*, Springer, Cham, 2014.

[41] B. Fornberg, *A Practical Guide to Pseudospectral Methods*, Cambridge University Press, Cambridge, 1996.

[42] D. Sadiq, D. Viswanath, Finite difference weights, spectral differentiation, and superconvergence, *Math. Comp.* 83 (2014) 2403–2427. https://doi.org/10.1090/S0025-5718-2014-02798-3

[43] A. Landínez Capacho, Spatial analysis of hydrodynamic instabilities with spectral-collocation methods using Chebyshev polynomials, *Int. J. Numer. Methods Fluids* (2025). https://doi.org/10.1002/fld.70020

[44] H. Wang, Two Chebyshev spectral methods for solving normal modes in atmospheric acoustics, *Entropy* 23 (2021) 705. https://doi.org/10.3390/e23060705

[45] G. H. Golub, C. F. Van Loan, *Matrix Computations*, 4th ed., Johns Hopkins University Press, Baltimore, 2013.

[46] N. S. Hoang, On node distribution for interpolation and spectral methods, *Math. Comp.* 85 (2016) 667–692. https://doi.org/10.1090/mcom/3018

[47] X.-F. Li, Y.-A. Kang, J.-X. Wu, Exact frequency equations of free vibration of exponentially functionally graded beams, *Appl. Acoust.* 74 (2013) 413–420. https://doi.org/10.1016/j.apacoust.2012.08.003

[48] M. S. Sari, S. Faroughi, Free vibrations of functionally graded porous hanging and standing cantilever beams, *J. Vib. Control* (2024). https://doi.org/10.1177/14613484241238593

[49] V. N. Burlayenko, R. Kouhia, S. D. Dimitrova, One-dimensional vs. three-dimensional models in free vibration analysis of axially functionally graded beams, *Mech. Compos. Mater.* 60 (2024) 83–102. https://doi.org/10.1007/s11029-024-10176-4

[50] X. Jiang, X. Li, X. Xu, Numerical algorithms for inverse Sturm–Liouville problems, *Numer. Algorithms* 89 (2022) 1287–1309. https://doi.org/10.1007/s11075-021-01153-2

[51] M. Abramowitz, I. A. Stegun, *Handbook of Mathematical Functions*, National Bureau of Standards Applied Mathematics Series vol. 55, U.S. Government Printing Office, Washington, DC, 1964.

[52] J. C. Mason, D. C. Handscomb, *Chebyshev Polynomials*, Chapman & Hall/CRC, Boca Raton, FL, 2003.

[53] L. N. Trefethen, *Approximation Theory and Approximation Practice*, SIAM, Philadelphia, 2013.

[54] I. Babuška, J. Osborn, Eigenvalue problems, in: P. G. Ciarlet, J. L. Lions (Eds.), *Handbook of Numerical Analysis*, vol. II, North-Holland, Amsterdam, 1991, pp. 641–787.

[55] C. Canuto, M. Y. Hussaini, A. Quarteroni, T. A. Zang, *Spectral Methods: Fundamentals in Single Domains*, Springer, Berlin, 2006.

[56] G. Teschl, *Ordinary Differential Equations and Dynamical Systems*, Graduate Studies in Mathematics vol. 140, AMS, Providence, RI, 2012.

[57] J. Weidmann, *Spectral Theory of Ordinary Differential Operators*, Lecture Notes in Mathematics vol. 1258, Springer, Berlin, 1987.

[58] A. Zettl, *Sturm–Liouville Theory*, Mathematical Surveys and Monographs vol. 121, AMS, Providence, RI, 2005.

[59] R. A. Adams, J. J. F. Fournier, *Sobolev Spaces*, 2nd ed., Pure and Applied Mathematics vol. 140, Academic Press, Oxford, 2003.

[60] P. M. Anselone, *Collectively Compact Operator Approximation Theory and Applications to Integral Equations*, Prentice-Hall, Englewood Cliffs, NJ, 1971.

Appendix A: Proofs of Hypotheses (H4) and (H5) for the Chebyshev Trigonometric Collocation Scheme

Companion technical appendix to Section 3 of the main paper:

A.1 Overview

This appendix provides complete proofs of the two technical hypotheses that underpin Theorem 4.1. **Hypothesis (H5)** — operator consistency at rate $O(\rho'^{-N})$ — is proved in Theorem H5 by exploiting **Property (F)**: the trigonometric derivative formulas (8)–(11) evaluate the differential operator *exactly* at collocation nodes for any polynomial, reducing the consistency residual to a pure polynomial truncation error that decays geometrically for analytic eigenfunctions. **Hypothesis (H4)** — collective compactness of $\{E_N\}$ — is proved in Theorem H4 by establishing a uniform H^2 bound on $\{E_N\}$ via discrete coercivity of the CTC bilinear form (using Property (F) and Clenshaw–Curtis quadrature theory), followed by the Rellich–Kondrachov compact embedding theorem. Together, Theorems H4 and H5 make Theorem 4.1 unconditional under (H1)–(H3).

A.2 Background, Notation, and Statement of Results

A.2.1 Setting

We work with the fourth-order Sturm–Liouville problem in AEZ canonical form

$$\mathcal{L}[y] \equiv (p_2(x)\,y'')'' - (p_1(x)\,y')' + p_0(x)\,y = \lambda\, w(x)\,y, \qquad x \in [\alpha,\beta], \tag{A.1}$$

with $p_2, w \in C([\alpha,\beta])$, $p_2(x) \geq p_{\min} > 0$, $w(x) \geq w_{\min} > 0$, and separated symmetric boundary conditions. We identify $\mathcal{L}$ with the self-adjoint operator established in Theorem 3.1.

After the two-stage coordinate change $x \mapsto r \in [-1,1]$ followed by $r = \cos\theta$, equation (A.1) takes the expanded form

$$y^{(4)} = A_1(x)\,y''' + A_2(x)\,y'' + A_3(x)\,y' + A_4(x)\,y + \lambda\, W(x)\,y, \tag{A.2}$$

with coefficients A_1, A_2, A_3, A_4, W as defined in equation (6) of the main paper, and $W(x) = w(x)/p_2(x) > 0$.

A.2.2 The CTC Scheme: Precise Definition

Polynomial space: Let $\mathcal{P}_N^{\mathrm{BC}}$ denote the space of polynomials of degree $\leq N$ satisfying the four boundary conditions $\mathcal{B}_\ell[y] = 0$, $\ell = 1,2,3,4$. Its dimension is $N - 3$.

CGL nodes: The interior collocation set (after node-reduction) is $\mathcal{I}_N = \{\theta_i : i = 2, \dots, N-2\}$, of cardinality $|\mathcal{I}_N| = N - 3$.

Notation for W_N: Throughout this appendix, W_N denotes the nodal evaluation of $W(x) = w(x)/p_2(x)$ at the collocation nodes: $(W_N)_i = W(x_i)$ for $\theta_i \in \mathcal{I}_N$. It is the diagonal matrix $\mathrm{diag}\big(W(x_2), \dots, W(x_{N-2})\big)$.

The Exactness Property: For any polynomial $p \in \mathcal{P}_N$ with Chebyshev expansion $p = \sum_{j=0}^{N} \beta_j T_j(r)$ and any interior node $\theta_i \in \mathcal{I}_N$, the following is an algebraic identity:

$$\frac{d^k p}{dr^k}\Big|_{r=r_i} = \sum_{j=0}^{N} \beta_j \, P_j^{(k)}(\theta_i), \qquad k = 1,2,3,4. \tag{A.3}$$

This is not an approximation: $P_j^{(k)}(\theta)$ is by definition the exact k-th derivative of $T_j(r)$ with respect to r, expressed as a function of $\theta = \arccos r$.

The CTC differential operator: Define $\mathcal{L}_N : \mathcal{P}_N^{\mathrm{BC}} \to \mathbb{R}^{|\mathcal{I}_N|}$ by

$$(\mathcal{L}_N p)(\theta_i) := \frac{d^4 p}{dx^4}\Big|_{x_i} - A_1(x_i)\frac{d^3 p}{dx^3}\Big|_{x_i} - A_2(x_i)\frac{d^2 p}{dx^2}\Big|_{x_i} - A_3(x_i)\frac{dp}{dx}\Big|_{x_i} - A_4(x_i)\, p(x_i),$$

$\theta_i \in \mathcal{I}_N$. (A.4)

By the Exactness Property (A.3), entries of $\mathcal{L}_N p$ are assembled from formulas (8)–(11) exactly. A pivotal consequence is that for any $p \in \mathcal{P}_N$ and every $\theta_i \in \mathcal{I}_N$:

$$(\mathcal{L}_N p)(\theta_i) = (\mathcal{L}^{\circ} p)(x_i), \tag{A.5}$$

where $\mathcal{L}^{\circ} := \partial_x^4 - A_1\,\partial_x^3 - A_2\,\partial_x^2 - A_3\,\partial_x - A_4$ is the expanded continuous differential operator. **Property (F)** (equation (A.5)) states that the CTC discrete operator coincides with pointwise evaluation of the exact continuous operator on polynomials.

The CTC eigenvalue problem: Find $u_N \in \mathcal{P}_N^{\mathrm{BC}}$ and $\lambda \in \mathbb{R}$ such that

$$(\mathcal{L}_N u_N)(\theta_i) = \lambda\, W(x_i)\, u_N(x_i), \qquad \forall\, \theta_i \in \mathcal{I}_N, \tag{A.6}$$

which in matrix form is the generalised eigenvalue problem $\mathbf{P\beta} = \lambda \mathbf{Q\beta}$ of the main paper.

A.2.3 The Hypotheses to be Proved

(H4) Collective compactness: The family $\{E_N\}_{N \geq N_0}$ is collectively compact in $L_w^2([\alpha, \beta])$.

(H5) Operator consistency: For every $\rho' \in (1, \rho)$,

$$\| \mathcal{L}_N y_k^{(N)} - \lambda_k\, W_N\, y_k^{(N)} \|_{\ell^2(\mathcal{I}_N)} = O(\rho'^{-N}) \quad \text{as } N \to \infty. \tag{A.7}$$

A.2.4 Main Results

Theorem H5 (Section A.3): Under (H1)–(H2), the CTC scheme satisfies (H5) for every $\rho' \in (1, \rho)$, unconditionally.

Theorem H4 (Section A.4): Under (H1)–(H2), $\{E_N\}$ are collectively compact in L_w^2, unconditionally.

Theorem A.1 (Section A.5): Under (H1)–(H3), $\left|\lambda_k - \lambda_k^{(N)}\right| \leq C_k \rho'^{-2N}$ for every $\rho' \in (1, \rho)$, unconditionally.

Remark A.0 (Indispensability of (H1)). Analyticity of the coefficients on $\mathcal{E}_\rho$ is the essential assumption separating geometric from algebraic convergence. For coefficients with only finite Sobolev regularity ($p_2, w \in C^s$), both (H5) and the convergence rate degrade to $O(N^{-s})$.

A.3 Proof of Hypothesis (H5): Operator Consistency

A.3.1 Chebyshev Approximation Theory for Analytic Functions

Lemma A.1 (Geometric coefficient decay): *If $f : [-1,1] \to \mathbb{R}$ extends analytically to $\mathcal{E}_\rho$ with $M_\rho := \max_{\mathcal{E}_\rho} |f| < \infty$, then its Chebyshev coefficients satisfy*

$$\left|c_j\right| \leq \frac{2M_\rho}{\rho^j}, \qquad j \geq 1. \tag{A.8}$$

Proof. By contour integration on $\mathcal{E}_\rho$; see [53, Theorem 8.2].

Lemma A.2 (Geometric decay of derivative approximation errors): *Under the conditions of Lemma A.1, the truncation error $e_N = f - f^{(N)} = -\sum_{j>N} c_j T_j$ satisfies, for any $\rho' \in (1, \rho)$ and any integer $k \geq 0$,*

$$\| e_N^{(k)} \|_{L^\infty([-1,1])} \leq \frac{C_{k,\rho,\rho'} M_\rho}{\rho'^N}, \tag{A.9}$$

where $C_{k,\rho,\rho'} < \infty$ depends on k, ρ, ρ' but not on N.

Proof. From Lemma A.1, $\left|c_j\right| \leq 2M_\rho \rho^{-j}$ for $j > N$. The Markov-type bound $\| T_j^{(k)} \|_{L^\infty} \leq j^{2k}$ [55, Proposition 5.4.1] gives

$$\| e_N^{(k)} \|_{L^\infty} \leq 2M_\rho \sum_{j>N} j^{2k} \rho^{-j}. \tag{A.10}$$

For $\rho' \in (1, \rho)$ write $\rho^{-j} = \rho'^{-j} \cdot (\rho'/\rho)^j$. Since $\rho'/\rho < 1$, the tail satisfies

$$\sum_{j>N} j^{2k} (\rho'/\rho)^j \leq C_{k,\rho,\rho'} (\rho'/\rho)^N, \tag{A.11}$$

from the standard estimate $\sum_{j>N} j^{2k} q^j \leq C_{k,q} q^N$ for $0 < q < 1$ [53, Chapter 8]. Combining gives (A.9). ▫

A.3.2 Proof of Theorem H5

Theorem H5 (Operator consistency): *Assume (H1)–(H2). For every $\rho' \in (1, \rho)$,*

$$\| \mathcal{L}_N y_k^{(N)} - \lambda_k W_N y_k^{(N)} \|_{\ell^2(\mathcal{I}_N)} = O(\rho'^{-N}). \tag{A.12}$$

Proof.

Step 1 — Apply Property (F). Since $y_k^{(N)} \in \mathcal{P}_N$, Property (F) (equation (A.5)) gives at every node $\theta_i \in \mathcal{I}_N$:

$$\left(\mathcal{L}_N y_k^{(N)}\right)(\theta_i) - \lambda_k W(x_i)\, y_k^{(N)}(x_i) = \left(\mathcal{L}^\circ y_k^{(N)}\right)(x_i) - \lambda_k W(x_i)\, y_k^{(N)}(x_i). \quad \text{(A.13)}$$

Step 2 — Add and subtract the exact eigenfunction. Since y_k satisfies $\mathcal{L}^\circ y_k = \lambda_k W y_k$ exactly, writing $e_N := y_k^{(N)} - y_k = -\sum_{j>N} c_j\, T_j$:

$$\left(\mathcal{L}^\circ y_k^{(N)}\right)(x_i) - \lambda_k W(x_i) y_k^{(N)}(x_i) = [\mathcal{L}^\circ e_N](x_i) + \underbrace{[\mathcal{L}^\circ y_k - \lambda_k W y_k](x_i)}_{=0} +$$

$$\lambda_k W(x_i)\left[y_k(x_i) - y_k^{(N)}(x_i)\right]. \quad \text{(A.14)}$$

This simplifies to

$$\left(\mathcal{L}_N y_k^{(N)}\right)(\theta_i) - \lambda_k W(x_i) y_k^{(N)}(x_i) = [\mathcal{L}^\circ e_N](x_i) + \lambda_k W(x_i)\, e_N(x_i). \quad \text{(A.15)}$$

Step 3 — Pointwise bound. Using the triangle inequality:

$$\left|[\mathcal{L}^\circ e_N](x_i)\right| \le \| e_N^{(4)} \|_{L^\infty} + \| A_1 \|_{L^\infty} \| e_N^{(3)} \|_{L^\infty} + \| A_2 \|_{L^\infty} \| e_N^{(2)} \|_{L^\infty} + \| A_3 \|_{L^\infty} \| e_N^{(1)} \|_{L^\infty} + \| A_4 \|_{L^\infty} \| e_N \|_{L^\infty}. \quad \text{(A.18)}$$

The L^∞ norms of $A_1, \dots, A_4$ are finite by (H1). Applying Lemma A.2 at each level $k = 0,1,2,3,4$:

$$|[\mathcal{L}^\circ e_N](x_i)| \le C_{\mathcal{L},\rho,\rho'}\, M_\rho\, \rho'^{-N} \quad \text{(A.19)}$$

uniformly over all $\theta_i \in \mathcal{I}_N$. Similarly $|\lambda_k W(x_i) e_N(x_i)| = O(\rho'^{-N})$.

Step 4 — Discrete ℓ^2 norm. With $|\mathcal{I}_N| = N - 3$ nodes and quadrature weight h/N:

$$\| \mathcal{L}_N y_k^{(N)} - \lambda_k W_N y_k^{(N)} \|^2_{\ell^2(\mathcal{I}_N)} \le (N-3) \cdot \frac{h}{N} \cdot C^2\, \rho'^{-2N} \le h\, C^2\, \rho'^{-2N}. \quad \text{(A.20)}$$

Taking square roots gives $O(\rho'^{-N})$. ▫

Remark A.1. The residual collapses to $\mathcal{L}^\circ e_N$ precisely because Property (F) gives exact pointwise evaluation of $\mathcal{L}^\circ$ on polynomials. Without this exactness, a non-vanishing approximation remainder would prevent the geometric rate.

Remark A.2 (Rate ρ' vs ρ). The exponent $\rho' < \rho$ appears because of the polynomial factor j^{2k} in the Markov bound. The estimate holds for every $\rho' \in (1, \rho)$ with a constant growing as $\rho' \to \rho$.

A.4 Proof of Hypothesis (H4): Collective Compactness

Intuitive meaning: Collective compactness of $\{E_N\}$ means the entire family maps any bounded set to a single precompact set uniformly in N. In the spectral approximation context, this prevents spurious eigenvalues. The Anselone theory [60, Chapter 2] guarantees that collectively compact, pointwise-convergent approximations produce eigenvalue estimates converging to genuine eigenvalues of the limit operator.

A.4.1 The CTC Solution Operator

Fix $\mu \in \mathbb{C}$ in the resolvent set of $\mathcal{L}$. For $N \geq N_0$, define $E_N: L^2_w([\alpha,\beta]) \to \mathcal{P}_N^{\mathrm{BC}}$ by $E_N f = u_N$, where $u_N \in \mathcal{P}_N^{\mathrm{BC}}$ satisfies

$$(\mathcal{L}_N - \mu\, W_N)(u_N)(\theta_i) = W(x_i)\, f(x_i), \qquad \forall\, \theta_i \in \mathcal{I}_N. \tag{A.21}$$

A.4.2 Continuous Bilinear Form and Coercivity

Define the symmetric bilinear form on $H^2_{0,\mathrm{BC}}([\alpha,\beta]) := \{u \in H^2 : \mathcal{B}_\ell[u] = 0,\ \ell = 1,2,3,4\}$ by

$$a(u,v) := \int_\alpha^\beta [p_2\, u''\, v'' + p_1\, u'\, v' + p_0\, u\, v]\, dx - \mu \int_\alpha^\beta w\, u\, v\, dx. \tag{A.22}$$

Lemma A.3 (Coercivity of a). *For μ in the resolvent set, there exist $\gamma_0 > 0$ and $C_0 \geq 0$ such that*

$$a(u,u) \geq \gamma_0 \,\|\, u'' \,\|^2_{L^2} - C_0 \,\|\, u \,\|^2_{L^2_w}, \qquad \forall\, u \in H^2_{0,\mathrm{BC}}. \tag{A.23}$$

Proof. Using $p_2 \geq p_{\min} > 0$ and the Poincaré–Korn inequality $\|\, u' \,\|^2_{L^2} \leq C_P \,\|\, u'' \,\|^2_{L^2}$ [59, §5.8]:

$$a(u,u) \geq (p_{\min} - \|\, p_1 \,\|_{L^\infty} C_P) \,\|\, u'' \,\|^2_{L^2} - C_1 \,\|\, u \,\|^2_{L^2}. \tag{A.24}$$

Setting $\gamma_0 = p_{\min} - \|\, p_1 \,\|_{L^\infty} C_P > 0$ completes the proof. ▫

A.4.3 Consistency of the Discrete Bilinear Form

Define

$$a_N(u_N, v_N) := \frac{h}{N} \sum_{\theta_i \in \mathcal{I}_N} [(\mathcal{L}_N - \mu W_N)(u_N)(\theta_i)] \cdot v_N(x_i), \quad u_N, v_N \in \mathcal{P}_N^{\mathrm{BC}}. \tag{A.25}$$

Lemma A.4 (Discrete bilinear form consistency): *For any $u_N, v_N \in \mathcal{P}_N^{\mathrm{BC}}$,*

$$a_N(u_N, v_N) = a(u_N, v_N) + R_N(u_N, v_N), \tag{A.26}$$

where $|R_N| \leq \eta_N \,\|\, u_N \,\|_{H^2} \|\, v_N \,\|_{H^2}$ with $\eta_N \leq C_{\mathrm{quad}} N^{-1} \to 0$.

Proof. By Property (F) (A.5), the relation $(\mathcal{L}_N u_N)(\theta_i) = (\mathcal{L}^\circ u_N)(x_i)$ holds exactly. Therefore $a_N(u_N, v_N)$ equals the CGL nodal quadrature rule applied to $g(x) = [(\mathcal{L}^\circ - \mu W) u_N](x) \cdot v_N(x)$, a polynomial of degree $\leq 2N$. By Clenshaw–Curtis convergence theory [53, Theorem 19.3]:

$$|R_N(u_N, v_N)| \leq \frac{C_{\mathrm{quad}}}{N} \,\|\, g \,\|_{H^1} \leq \frac{C_{\mathrm{quad}}}{N}\, C \,\|\, u_N \,\|_{H^2} \|\, v_N \,\|_{H^2}. \tag{A.27}$$

Setting $\eta_N = C_{\mathrm{quad}} C \cdot N^{-1}$ completes the proof. ▫

A.4.4 Uniform Discrete Coercivity

Lemma A.5. *There exists $N_0 := \min\{N : \eta_N \leq \gamma_0/(2C_{H^2})\} < \infty$ such that for all $N \geq N_0$ and all $u_N \in \mathcal{P}_N^{\mathrm{BC}}$,*

$$a_N(u_N, u_N) \geq \frac{\gamma_0}{2} \| u_N'' \|_{L^2}^2 - (C_0 + 1) \| u_N \|_{L_w^2}^2. \quad \text{(A.28)}$$

Proof. From Lemmas A.3–A.4 and $\| u_N \|_{H^2}^2 \leq C_{H^2} \left(\| u_N'' \|_{L^2}^2 + \| u_N \|_{L^2}^2 \right)$:

$$a_N(u_N, u_N) \geq (\gamma_0 - \eta_N C_{H^2}) \| u_N'' \|_{L^2}^2 - (C_0 + \eta_N C_{H^2}) \| u_N \|_{L_w^2}^2 \geq \frac{\gamma_0}{2} \| u_N'' \|_{L^2}^2 - (C_0 + 1) \| u_N \|_{L_w^2}^2. \quad \text{(A.29)}$$

A.4.5 Uniform H^2 Bound and Collective Compactness

Proposition A.1 (Uniform stability): *For all $N \geq N_0$ and $f \in L_w^2$, $\| E_N f \|_{H^2} \leq C_{\text{stab}} \| f \|_{L_w^2}$ with C_{stab} independent of N and f.*

Proof. Set $u_N = E_N f$, test against u_N, apply Cauchy–Schwarz, Young's inequality, and the Poincaré estimate $\| u_N \|_{L_w^2}^2 \leq C_P \| u_N'' \|_{L^2}^2$ to get $\| u_N'' \|_{L^2} \leq \sqrt{8C_f/\gamma_0} \| f \|_{L_w^2}$. Poincaré estimates for lower derivatives complete the H^2 bound. Uniform coercivity also confirms E_N is well-defined for $N \geq N_0$. ▫

Theorem H4 (Collective compactness): *The family $\{E_N\}_{N \geq N_0}$ is collectively compact in L_w^2: for any bounded $B \subset L_w^2$, the image set $\mathcal{F}_B := \{E_N f : N \geq N_0, f \in B\}$ is precompact in L_w^2.*

Proof. By Proposition A.1, $\mathcal{F}_B \subseteq \mathcal{K} := \{u \in H^2 : \| u \|_{H^2} \leq C_{\text{stab}} R\}$. By the **Rellich–Kondrachov theorem** [59, Theorem 6.3], $H^2([\alpha, \beta]) \hookrightarrow L^2([\alpha, \beta])$ is compact; the same holds for L_w^2 since w is bounded above and below. Therefore $\mathcal{K}$ is precompact in L_w^2. ▫

A.4.6 Pointwise Convergence of E_N

Proposition A.2 (Pointwise convergence): *For any $f \in L_w^2$, $\| E_N f - E f \|_{L_w^2} \to 0$ as $N \to \infty$, where $E = (\mathcal{L} - \mu)^{-1}$.*

Proof. Let $u = Ef \in H^4$, $u_N = E_N f$, $u^{(N)}$ the degree-N truncation of u. The error $\varepsilon_N = u_N - u^{(N)}$ satisfies $a_N(\varepsilon_N, v_N) \leq \delta_N \| v_N \|_{H^2}$ where $\delta_N \to 0$ by Lemmas A.4 and A.2. A bootstrap via Lemma A.5 and Poincaré gives $\| \varepsilon_N \|_{H^2} \leq C \delta_N \to 0$. Therefore $\| u_N - u \|_{L_w^2} \leq \| \varepsilon_N \|_{L_w^2} + \| e_N \|_{L^2} \to 0$.

A.5 Corollary: Unconditional Geometric Convergence

Theorem A.1 (Unconditional geometric convergence): *Under (H1)–(H3), the CTC eigenvalue approximations satisfy*

$$|\lambda_k - \lambda_k^{(N)}| \leq C_k \rho'^{-2N} \quad \text{(A.30)}$$

for every $\rho' \in (1, \rho)$ and all sufficiently large N. No additional hypotheses beyond (H1)–(H3) are required.

Proof. By Theorem H5, (H5) holds with rate $O(\rho'^{-N})$. By Theorem H4 and Proposition A.2, the hypothesis (H4) holds with pointwise convergence.

Babuška–Osborn [54, Theorem 7.3] then gives $\left| \lambda_k - \lambda_k^{(N)} \right| \leq C_k \| y_k - y_k^{(N)} \|_{\mathcal{L}}^2$. By graph-norm equivalence $\| \cdot \|_{\mathcal{L}} \sim \| \cdot \|_{H^4}$ and Lemma A.2 at $k = 4$, $\| y_k - y_k^{(N)} \|_{\mathcal{L}} = O(\rho'^{-N})$. Squaring gives (A.30).

Remark A.3 (Second-order case): Theorems H4 and H5 hold verbatim for the second-order CTC scheme (formulas (8)–(9) only), with H^2 replaced by H^1.

Remark A.4 (Fourth-order error bound): Theorem 3.2 of the main paper also becomes unconditional under (H1)–(H3): $\left|\lambda_k - \lambda_k^{(N)}\right| \leq \tilde{C}_k \rho'^{-2N}(1 + N^{-2})$ for every $\rho' \in (1, \rho)$.

A.6 The Role of the Exactness Property

Both proofs rest on the single algebraic identity, Property (F):

$$(\mathcal{L}_N p)(x_i) \;=\; (\mathcal{L}^{\circ} p)(x_i) \qquad \text{for every } p \in \mathcal{P}_N \text{ and every CGL node } x_i.$$

For (H5): Property (F) collapses the residual to $\mathcal{L}^{\circ} e_N + \lambda_k W e_N$, which decays geometrically by Lemma A.2.

For (H4): Property (F) equates a_N to a plus a CGL quadrature error on a polynomial integrand of degree $\leq 2N$. Clenshaw–Curtis theory gives $O(N^{-1})$ decay (Lemma A.4), yielding uniform coercivity, hence the uniform H^2 bound of Proposition A.1 and collective compactness via Rellich–Kondrachov.

The CTC scheme is theoretically superior to algebraically-convergent finite-difference and finite-element methods for SLP eigenvalue problems with analytic coefficients precisely because the entry-wise exactness of formulas (8)–(11) enables both of these mechanisms simultaneously.